Gas-Phase Nuclear Magnetic Resonance Study of Berry Pseudorotation of SF_4. Comparison of Experimental and Calculated Kinetic Parameters and Falloff Kinetics

Angela N. Taha,[†] Nancy S. True,*[,†] Clifford B. LeMaster,[‡] Carole L. LeMaster,[‡] and Susan M. Neugebauer-Crawford[§]

Department of Chemistry, University of California, One Shields Avenue, Davis, California 95616, Department of Chemistry, Boise State University, Boise, Idaho 83725, and Department of Chemistry, California State University, Sacramento, California 95819

Received: November 10, 1999; In Final Form: February 9, 2000

Temperature-dependent Berry pseudorotation rate constants of SF_4 gas at ca. 7.9 atm, determined from analysis of exchange-broadened ^{19}F NMR spectra, are consistent with $E_\infty = 11.9(0.2)$ kcal mol^{-1}, $A_\infty = 3.56(1.09) \times 10^{12}$ s^{-1}, $\Delta G^{\ddagger}_{298} = 12.2(0.1)$ kcal mol^{-1}, $\Delta H^{\ddagger}_{298} = 11.3(0.4)$ kcal mol^{-1}, and $\Delta S^{\ddagger}_{298} = -3.3(0.4)$ cal mol^{-1} K^{-1}. Using a 6-31+G* basis set, HF calculations predict $\Delta H^{\ddagger}_{298} = 12.26$ kcal mol^{-1} and $\Delta S^{\ddagger}_{298} = -3.74$ cal mol^{-1} K^{-1} and MP2 calculations predict $\Delta H^{\ddagger}_{298} = 9.99$ kcal mol^{-1} and $\Delta S^{\ddagger}_{298} = -3.89$ cal mol^{-1} K^{-1}. Stationary point MP4/6-31+G*//HF/6-31+G* calculations predict $\Delta H^{\ddagger}_{298} = 11.55$ kcal mol^{-1} and $\Delta S^{\ddagger}_{298} = -3.91$ cal mol^{-1} K^{-1}. DFT calculations using the 6-31+G* basis set and the B3LYP and B3PW91 hybrid functionals are considerably less accurate. Pressure-dependent rate constants obtained at 335 K agree well with RRKM theory predictions using the strong collision assumption. The curvature and displacement of the experimental falloff curve are not significantly perturbed by effects of weak collisions and/or nonstatistical intramolecular vibrational energy redistribution.

Introduction

SF_4 is one of the smallest molecules that undergoes an intramolecular rearrangement which has rate constants accessible to NMR measurement.[1] The Berry pseudorotation process of SF_4 concertedly exchanges the magnetically inequivalent sets of axial and equatorial fluorine atoms.[2] Of the many low-energy intramolecular exchange processes which we have studied in the gas phase using NMR spectroscopy,[3−5] this is the only one which appeared to exhibit non-RRKM kinetics. Our 1983 gas-phase NMR study of SF_4 concluded that pressure-dependent rate constants between 55 and 2005 Torr could not be modeled adequately using RRKM theory.[6] In that study, plots of RRKM calculated reduced rate constants, k/k_∞, were found to have greater curvature and were displaced to higher pressures than the experimentally determined k/k_∞ values. Bauer et al. also concluded that the kinetics of SF_4 Berry pseudorotation was non-RRKM because k_{uni}/P increased with decreasing pressure for the low-pressure data obtained in our study, which is not consistent with RRKM predictions for bimolecular rate constants.[7] Non-RRKM kinetics appeared reasonable for SF_4 Berry pseudorotation. State densities are sparse at the low energies required for the process and intramolecular vibrational redistribution (IVR) may not be ergodic, thus violating a key assumption of all statistical kinetic theories.[8]

Our previous SF_4 study was one of the first gas-phase NMR studies reported from our laboratory and did not benefit from the improvements in experimental design and theoretical modeling of subsequent studies. Gas samples used in that study were prepared in 8 in. long NMR tubes, and their spectra were obtained at temperatures above 300 K. These conditions result in convection within the sealed tubes which can cause inaccurate temperature measurements.[5] Our later kinetic studies used restricted volume NMR tubes to eliminate this problem.[3−5] The RRKM calculations performed used a set of vibrational frequencies for the transition state which were arbitrarily chosen to match the Arrhenius preexponential factor, *A*, obtained for a 2004 Torr sample of SF_4 gas. The present study shows that the kinetics of the pseudorotation process is not at its high pressure limit at 2004 Torr and the *A* factor obtained previously was too large, possibly due to a small systematic error in temperature measurement.

The accuracy of ab initio predictions of ground- and transition-state structures and vibrational frequencies has improved significantly since 1983. For example, high-level ab initio molecular orbital calculations successfully predicted gas-phase activation parameters for internal rotation of dimethylacetamide[9] and trifluoroacetamide.[10] Because the internal rotation processes of these molecules are statistical and data were obtained in the gas phase without solvent effects, experimental and calculated activation parameters are directly comparable. In both studies, the experimental and calculated activation entropies, $\Delta S^{\ddagger}$, agreed well. The agreement between experiment and theory indicates that structures and vibrational frequencies of transition states can be predicted with good accuracy with currently available computational methods.

The present study reinvestigates the kinetics of Berry pseudorotation of SF_4. Temperature-dependent rate constants for a sample containing 5977 Torr of SF_4 were used to determine a high-pressure activation energy, E_∞, and pressure-dependent rate constants were obtained between 1850 and 5977 Torr to better define the falloff curve. Ab initio molecular orbital calculations of structures, energies, and vibrational frequencies of the ground and transition states at the HF, MP2, and MP4 levels of theory were performed to characterize the transition state. This is the

[†] University of California.
[‡] Boise State University.
[§] California State University.

10.1021/jp993991f CCC: $19.00 © 2000 American Chemical Society
Published on Web 03/28/2000

first time that rigorous ab initio calculations have been performed to provide parameters for modeling the transition state for Berry pseudorotation of SF_4. The present study also investigates the predictions of density functional theory using the B3LYP and B3PW91 hybrid density functionals. Ab initio calculations using G2 procedures were reported for the C_{2v} ground state of SF_4.[11] Earlier molecular orbital calculations of the ground state and Berry pseudorotation transition state of SF_4 were performed at the STO-3G*, 4-31G*, and 6-31G* levels of theory.[12,13]

RRKM theory was used to calculate pressure-dependent rate constants with the aid of the theoretical predictions of the structure and vibrational frequencies of the transition state. Weak collision and non-RRKM effects on the curvature and position of the falloff region were also investigated.

Experiments and Calculations

NMR Spectroscopy and Rate Constants. Gas-phase SF_4 samples were prepared in restricted volume NMR tubes constructed from 3 cm long sections of Wilmad high-precision 12 mm o.d. coaxial inserts. Prior to filling, the sample tube and vacuum manifold were flushed with 50−100 Torr of SF_4 to remove any H_2O and HF. Small amounts of sodium fluoride were also added to remove HF. Samples were prepared by quantitative transfer of a mixture of SF_4 and $CFCl_3$ from a calibrated glass bulb. $CFCl_3$ (5−10 Torr) was added as a frequency reference. Cooled samples were torch sealed and immersed in liquid nitrogen. Final sample pressures were determined after correcting for any residual pressure after sealing. Samples with total pressures above 3500 Torr were similarly prepared in 12 mm o.d. heavy-walled Wilmad NMR tubes. Spectral data were acquired for each sample immediately after preparation to prevent problems due to sample decomposition. All spectra showed traces of SOF_2 (0.5%) and SSF_2 (0.3%).[14] Room-temperature decomposition studies showed that after 118 h the SF_4 concentration decreased to 80% of its initial value.

Gas-phase NMR spectra of SF_4 were acquired on a wide-bore GE NT-300 NMR spectrometer (^{19}F observation at 282.34 MHz) fitted with a Tecmag acquisition upgrade and equipped with a Bradley 12 mm ^{19}F probe. All measurements were made on spinning samples in unlocked mode. Acquisition parameters were as follows: pulse length, 33 μs (90° flip angle); delay time, 0.5 s; acquisition time, 204.8 ms. Typically 1000−5000 transients were collected and stored in 8K of memory to achieve a maximum signal-to-noise ratio of 45:1 after multiplication by an exponential line-broadening factor of 30 Hz. A sweep width of ±25 000 Hz was employed. The temperature was controlled with a 0.1 °C pyrometer and read after each acquisition. Temperature measurements were made using two copper−constantan thermocouples placed within an empty NMR tube. Using this technique, the temperature gradient within the active volume of the probe was found to be less than 0.2 K. Samples were allowed to thermally equilibrate for at least 10 min prior to sample acquisition.

Rate constants were calculated using the program DNMR5,[15] which uses a nonlinear least-squares regression analysis to obtain the best fit of the experimental NMR spectrum. The program was provided with limiting chemical shifts, transverse relaxation times, and the digitized NMR spectrum. The limiting chemical shift difference was measured for slow exchange spectra at several temperatures and pressures and was found to be constant, in agreement with previous reports.[6,14] The natural line widths of the axial and equatorial fluorine resonances at all the pressures studied exceed the reported axial−equatorial coupling constant, 76.3 Hz.[20] Therefore, all spectra were analyzed using an uncoupled AX spin system model. The effective line width parameters for the axial and equatorial fluorines were measured at slow and fast exchange for each pressure sample and estimated in the exchange region by assuming a linear temperature dependence. The slow exchange natural line widths of the axial fluorines are greater than those of the equatorial fluorines, consistent with previously reported, T_1 values and spin−rotation coupling constants.[33] Rate constants in the exchange region were obtained by iterating on rate constant, spectral origin, baseline height, and baseline tilt. All other parameters were held constant.

Ab Initio Molecular Orbital Calculations. Ab initio molecular orbital calculations were performed on Gateway microcomputers using the Windows version of Gaussian 94.[16] Calculations were performed at the Hartree−Fock (HF), DFT (B3-PW91 and B3-LYP), MP2, MP4, and G2(MP2) theory levels using the 6-31+G* basis set. Additional DFT calculations were also performed using the 6-31G* basis set. All DFT calculations were performed using the fine integration grid.

RRKM Calculations. Calculations were performed using the RRKM program written by Hase and Bunker[17] as well as the RRKM program from the UNIMOL program suite of Gilbert, Smith, and Jordan.[18] Weak collision effects were investigated using MAS55 from the UNIMOL suite, which employs an energy-grained master equation.

Results and Discussion

Part 1 of this section reports NMR spectra, rate constants, and activation parameters for Berry pseudorotation of SF_4. Part 2 reports results of ab initio molecular orbital and DFT calculations of the energies, structures, and vibrational frequencies of the ground state and transition state for the Berry pseudorotation process of SF_4 and compares them with available experimental data and the activation parameters obtained in the present study. Part 3 describes RRKM calculations of pressure-dependent rate constants for this process and compares them with experimental data.

1. NMR Data and Rate Constants. Slow exchange spectra of gaseous SF_4 show two resonances centered at 93.74 and 32.84 ppm referenced to gas-phase $CFCl_3$ at 0.0 ppm which are assigned to the axial and equatorial fluorine atoms, respectively. These spectral assignments are consistent with our earlier report[6] and with theoretical chemical shift calculations.[19] Representative exchange-broadened gas-phase NMR spectra of a sample containing 5977 Torr of SF_4 are shown in Figure 1. Temperature-dependent rate constants obtained between 296.5 and 349.2 K, which are plotted in Figure 2, are consistent with $E_\infty = 11.9(0.2)$ kcal mol^{-1}, $A_\infty = 3.56(1.09) \times 10^{12}$ s^{-1}, $\Delta G^{\ddagger}_{298} = 12.2(0.1)$ kcal mol^{-1}, $\Delta H^{\ddagger}_{298} = 11.3(0.4)$ kcal mol^{-1}, and $\Delta S^{\ddagger}_{298} = -3.3(0.4)$ cal mol^{-1} K^{-1}. Our 1983 study reported $E_\infty = 13.7(0.5)$ kcal mol^{-1} for a 2004 Torr SF_4 sample. The most probable reason for the discrepancy is a systematic error in temperature measurement in the earlier study. In that study, exchange-broadened spectra were obtained between 298 and ca. 348 K. Convection currents occur in the sealed long tubes which were used since they are heated from the bottom and are cooler at the top of the tube which extends above the spinner. A higher E_{act} would result if the actual sample temperatures were lower than those measured, and the deviation increased with increasing temperature. Seel and Gombler reported E_a for a SF_4 gas sample at ca. 3500 Torr of 11.7(1.5) kcal mol^{-1}, very close to the value obtained in the present study.[20] Because they used a spectrometer

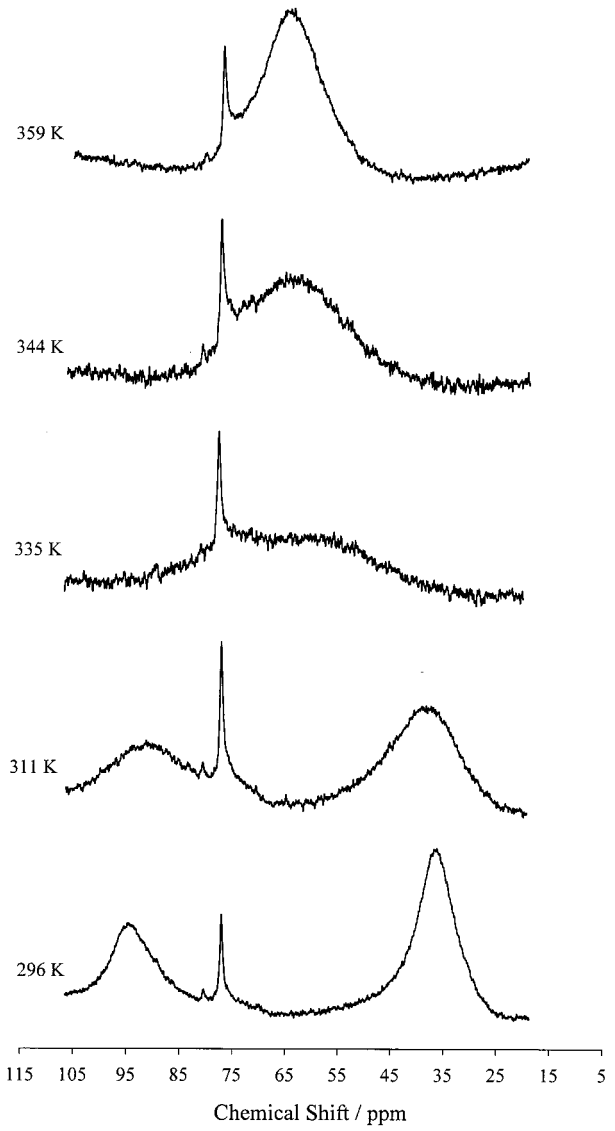

Figure 1. Gas-phase NMR spectra of a 5977 Torr sample of SF_4. Frequencies are referenced to gaseous $CFCl_3$ at 0.0 ppm. The broad resonance at 97 ppm is assigned to the axial fluorine atoms, and the resonance at 37 ppm is assigned to the equatorial fluorine atoms. The sharp resonance at 77 ppm is due to SOF_2 impurity, and the smaller resonance at 80 ppm is due to SSF_2 impurity.

with ^{19}F observation at 56.45 MHz, they obtained exchange-broadened spectra between 277 and 295 K where convection would not have been a problem.

The pressure-dependent rate constants reported in our earlier study were obtained between 50 and 2000 Torr.[6] In the present study we obtained rate constants between 1850 and 6000 Torr to better characterize the high-pressure region of the falloff curve, which is more sensitive to weak collision effects. Pressure-dependent rate constants obtained at 335.1 K in the present study are (P/Torr, k/s^{-1}) 1008, 49 680(1430); 1855, 60 620(1260); 2269, 62 130(930); 4558, 63 870(1140); 4780, 63 450(1350); 5322, 63 920(1050); and 5977, 64 170(1520).[21] These data were combined with the pressure-dependent rate constants obtained in our earlier study to obtain the falloff curve used for subsequent kinetic modeling.

2. Ab initio Calculations. Tables 1−4 summarize results of molecular orbital and DFT calculations of the energies, structures, and vibrational frequencies of the ground state and Berry pseudorotation transition state of SF_4 and the activation parameters for the pseudorotation process. Table 1 summarizes the nonscaled total and zero point energies of the ground and Berry pseudorotation transition state of SF_4 obtained from 10 calculations.

Ground-State SF_4. Inspection of Table 2 shows that rotational constants and structural parameters of SF_4 obtained from analysis of microwave spectra[22] agree well with values calculated at the HF/6-31+G* level. MP2/6-31+G*, G2(MP2), and the B3LYP and B3PW91 hybrid density functionals yield S−F bond lengths which are 0.04 Å longer, on average, than the experimental values. DFT methods tend to overestimate bond lengths,[23] but the deviations for SF_4 are much larger that those obtained for other small molecules which primarily consist of first- and second-row elements.[23] The electronegativity and polarizability differences between sulfur and fluorine are greater than those between the bonded atoms in the molecules examined in that study. This factor may contribute to the larger deviations in the DFT calculated bond lengths of SF_4. A systematic study of sulfur-containing molecules also concluded that DFT calculations poorly predict structural parameters.[24] Choice of basis set does appear to have a significant effect on the calculated bond lengths, with the 6-31+G* basis set yielding the largest values for both DFT methods. Overall, the B3PW91/6-31G** calculated geometry is closest to experiment. To investigate the applicability of DFT methods to other sulfur fluorides, B3LYP and B3PW91 calculations were also performed for SF and SF_2. These calculations predicted S−F bond lengths 0.03 Å longer than the experimental values for both SF and SF_2. The reliability of DFT methods for sulfur fluorides is far less superior than that of HF and MP2 methods.

The vibrational assignments listed in Table 3 agree with the most recent assignment reported by Irkura.[11] Scaling factors of 0.893 for HF, 0.943 for MP2 and MP4, and 0.961 for the hybrid density functionals provide the best agreement with the observed vibrational frequencies. The magnitudes of these scaling factors are close to recommended values.[25,26] Inspection of the atom displacements indicates that excitation of the lowest frequency A_1 normal mode results in progress along the Berry pseudorotation path, in agreement with the assignment of the far-infrared spectrum of SF_4.[27]

The G94 calculation at the HF/6-31+G* level predicts a ground-state entropy, S_{298}, of SF_4 of 69.488 cal mol^{-1} K^{-1}. Scaling the HF/6-31+G* vibrational frequencies by 0.893 increases S_{298} to 71.312 cal mol^{-1} K^{-1} in very good agreement with the experimental value, 70.72 cal mol^{-1} K^{-1}.[11] G94 S_{298} values at other theory levels, using appropriate vibrational frequency scaling factors, are slightly larger primarily due to larger rotational partition functions resulting from longer bond lengths. It should be noted that these experimental and G94 S_{298} values do not include the contribution to S due to the fact that the pseudorotation mode has a double minimum and its energy levels are doubly degenerate.

Calculated electric dipole moments of SF_4 are listed in Table 2. All the calculated values are larger than the experimental value, 0.632(0.003) D, determined from Stark effect measurements[22] of rotational transitions. Surprisingly, the B3LYP/6-31+G* and B3PW91/6-31+G* calculations with partial geometry optimization yield calculated dipole moments which are only slightly larger than the experimental value, while calculations at the HF/6-31+G*, MP2/6-31+G*, and G2(MP2) levels of theory yield much larger dipole moments.

Berry Pseudorotation Transition State of SF_4. Structural data and vibrational frequencies of the C_{4v} transition state for Berry pseudorotation of SF_4 are listed in Tables 2 and 3, respectively. All calculations predict the transition-state S−F bond length to

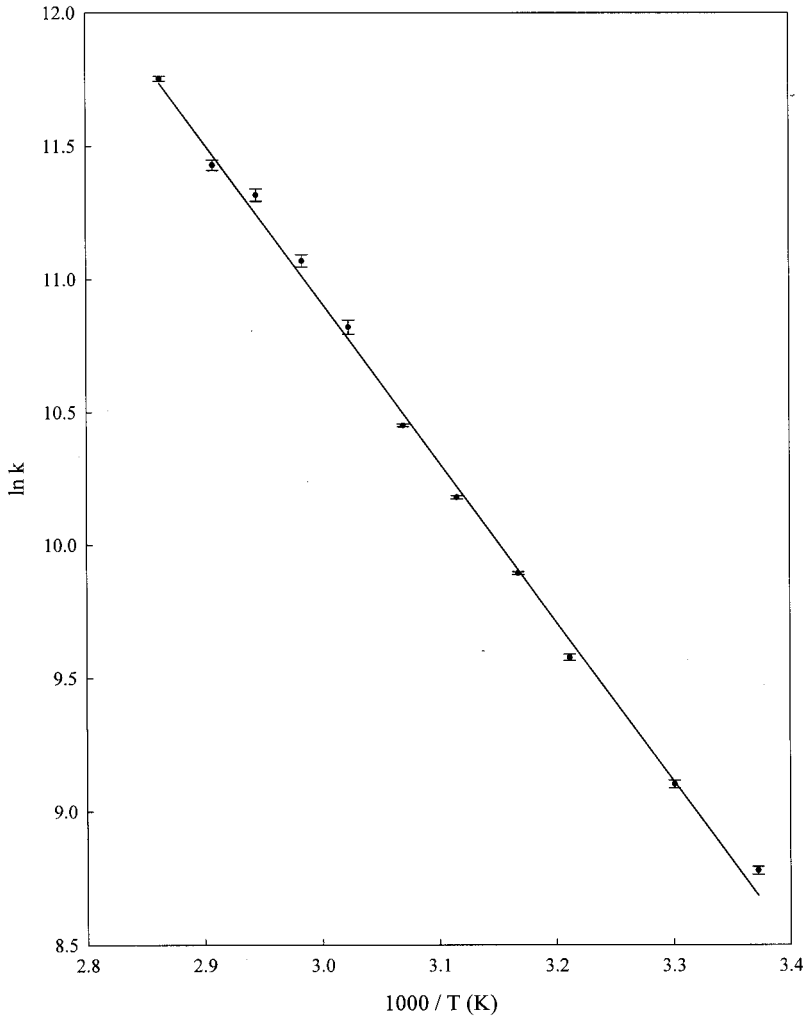

Figure 2. Temperature-dependent rate constants for Berry pseudorotation for a 5977 Torr sample of SF_4 gas. The experimental data are consistent: $E_\infty = 11.9(0.2)$ kcal mol^{-1}, $A_\infty = 3.56(1.09) \times 10^{12}$ s^{-1}, $\Delta G^{\ddagger}_{298} = 12.2(0.1)$ kcal mol^{-1}, $\Delta H^{\ddagger}_{298} = 11.3(0.4)$ kcal mol^{-1}, and $\Delta S^{\ddagger}_{298} = -3.3(0.4)$ cal mol^{-1} K^{-1}.

TABLE 1: Ab Initio and DFT Calculated Energies for Ground- and Transition-State Structures of SF_4[a]

	ground state		transition state	
method	energy	ZPE	energy	ZPE
HF/6-31+G*	−795.264 152 769	7.98	−795.244 491 705	7.89
MP2/6-31+G*	−796.258 485 469	7.20	−796.243 278 240	7.24
B3LYP/6-31+G*	−797.620 805 093	6.23	−797.607 432 759	6.56
B3LYP/6-31G**	−797.459 531 896	7.22	−797.448 073 862	7.21
B3PW91/6-31+G*	−797.406 572 500	6.79	−797.403 645 710	6.72
B3PW91/6-31G**	−797.267 595 422	7.12	−797.256 379 939	7.33
B3LYP/6-31+G* [b]	−797.611 987 773	7.54	−797.598 039 196	7.58
B3PW91/6-31+G* [b]	−797.410 505 654	7.58	−797.396 706 988	7.61
MP4/6-31+G*//HF/6-31+G*	−796.055 742 020	7.63	−796.037 276 110	7.59
MP4/6-31G**//B3LYP/6-31G**	−795.822 866 47	7.37	−795.806 625 361	7.36
G2(MP2)	−796.675 057	8.32	−796.657 249	8.29

[a] The nonscaled total and zero-point energies are in hartrees and in kcal mol^{-1}, respectively. [b] Partial geometry optimization with fixed atomic radii calculated at the HF/6-31+G* level of theory.

be ca. 0.01 Å larger than the average of the axial and equatorial bond lengths of the ground-state molecule. The lowest frequency vibrational mode has B_1 symmetry and is the reaction coordinate.[28] The entropy of the transition state, $S^{\ddagger}_{298}$, calculated at the HF/6-31+G* level, is 65.746 cal mol^{-1} K^{-1}, omitting the lowest frequency mode and using unscaled vibrational frequencies for the other normal modes. Scaling the calculated vibrational frequencies by 0.893 yields a $S^{\ddagger}_{298}$ of 66.837 cal mol^{-1} K^{-1}. Several factors contribute to the smaller $S^{\ddagger}_{298}$ of the transition state compared to that of the ground state. The lowest frequency vibration corresponds to the reaction coordinate and is excluded from the entropy calculation. Calculated vibrational frequencies for the transition state are all above 500 cm^{-1}, while the ground state has three vibrational frequencies below 500 cm^{-1}. Also, the rotational symmetry number of the C_{4v} transition state is 4, and that of the C_{2v} ground state is 2.

Comparison of the calculated activation parameters, listed in Table 4, with corresponding experimental values indicates better agreement at the HF, MP2, and MP4 levels than with DFT theory. The $\Delta S^{\ddagger}_{298}$ values[29] listed in Table 4 were calculated

TABLE 2: Ab Initio and DFT Calculated Molecular Geometries of Ground- (C_{2v}) and Transition-State (C_{4v}) Structures of SF_4[a]

	ground state					transition state	
method	r_{ax}	r_{eq}	$\angle FSF_{ax}$	$\angle FSF_{eq}$	dipole moment	r	$\angle$[b]
HF/6-31+G*	1.643	1.533	170.821	102.359	1.097	1.596	20.113
MP2/6-31+G*	1.689	1.578	172.392	101.953	1.263	1.645	19.828
B3LYP/6-31+G*	1.705	1.596	172.736	101.564	1.165	1.661	19.753
B3LYP/6-31G**	1.673	1.594	171.479	102.019	0.884	1.643	20.035
B3PW91/6-31+G*	1.693	1.589	172.512	101.715	1.091	1.651	19.749
B3PW91/6-31G**	1.665	1.588	171.311	102.084	0.852	1.636	20.021
B3LYP/6-31+G* [c]	1.643	1.533	173.768	101.544	0.761	1.596	19.395
B3PW91/6-31+G* [c]	1.643	1.533	173.529	101.659	0.733	1.596	19.429
G2(MP2)	1.663	1.585	175.552	102.014	1.021	1.635	20.169
experimental [d]	1.646(3)	1.545(3)	173.44(30)	101.33(30)	0.632(3)		

[a] Distances are given in angstroms, angles in degrees, and dipole moments in debyes. [b] The transition-state angle is defined as the angle of fluorine atoms bent out of the plane of the sulfur atom. [c] Partial geometry optimizations with fixed atomic radii calculated at the HF/6-31+G* level of theory. [d] Reference 21.

TABLE 3: Scaled Calculated Vibrational Frequencies for Ground- and Transition-State Structures of SF_4[a]

	ground state				transition state			
method	A1	A2	B1	B2	E[b]	A1	B1	B2
HF/6-31+G*	222, 518, 531, 867	455	520, 665	352, 856	505, 770	543, 775	166i, 524	541
MP2/6-31+G*	201, 503, 521, 852	458	317, 839	317, 839	461, 729	516, 738	141i, 494	503
B3LYP/6-31+G*	189, 451, 486, 776	397	455, 654	299, 745	449, 685	472, 709	131i, 474	482
B3LYP/6-31G**	181, 468, 562, 834	419	476, 776	318, 818	471, 789	505, 770	126i, 545	506
B3PW91/6-31+G*	192, 462, 500, 795	407	466, 672	308, 766	459, 706	484, 726	133i, 487	493
B3PW91/6-31G**	183, 476, 571, 848	425	484, 789	324, 833	477, 805	513, 782	129i, 555	513
B3LYP/6-31+G* [c]	178, 488, 579, 919	432	499, 762	304, 908	492, 833	510, 819	201i, 576	541
B3PW91/6-31+G* [c]	183, 493, 578, 919	435	502, 762	312, 910	496, 835	516, 820	196i, 576	542
MP4/6-31+G*//HF/6-31+G*	173, 500, 556, 894	447	509, 731	327, 896				
MP4/6-31G**//B3LYP/6-31G**	184, 470, 564, 831	418	474, 778	317, 826	470, 764	549, 792	133i, 507	506
experimental[d]	223, 475, 558, 892	414	532, 867	353, 730				

[a] Scaling factors are 0.893 for HF, 0.943 for MP2 and MP4, and 0.961 for hybrid density functionals. [b] Each vibrational mode doubly degenerate. [c] Partial geometry optimizations with fixed atomic radii calculated at the HF/6-31+G* level of theory. [d] Reference 11.

TABLE 4: Calculated Arrhenius Activation Energy and Eyring Activation Parameters at 298.15 K[a]

method	E_a	$\Delta G^{\ddagger}$	$\Delta H^{\ddagger}$	$\Delta S^{\ddagger}$
HF/6-31+G*	12.85	13.78	12.26	−3.74
MP2/6-31+G*	10.59	11.15	9.99	−3.89
B3LYP/6-31+G*	8.92	9.60	8.32	−4.29
B3LYP/6-31G**	7.77	8.49	7.18	−4.40
B3PW91/6-31+G*	9.02	9.69	8.43	−4.25
B3PW91/6-31G**	7.77	8.49	7.18	−4.40
B3LYP/6-31+G* [b]	9.33	10.11	8.74	−4.59
B3PW91/6-31+G* [b]	9.28	10.03	8.69	−4.50
MP4/6-31+G*//HF/6-31+G*	12.14	12.71	11.55	−3.91
MP4/6-31G**//B3LYP/6-31G**	10.77	11.47	10.18	−4.33
G2(MP2)	11.30	11.94	10.71	−4.11

[a] E_a, $\Delta G^{\ddagger}$, and $\Delta H^{\ddagger}$ in kcal mol^{-1} and $\Delta S^{\ddagger}$ in cal mol^{-1} K^{-1}. ZPE corrections are scaled by 0.893 for HF and G2(MP2), 0.943 for MP2 and MP4, and 0.961 for hybrid density functionals. [b] Partial geometry optimization with fixed atomic radii calculated at the HF/6-31+G* level of theory.

using unscaled vibrational frequencies. $\Delta S^{\ddagger}_{298}$ is not significantly different if appropriately scaled vibrational frequencies are used. For example, at the HF/6-31+G* level of theory, $\Delta S^{\ddagger}_{298}$ is −3.74 and −3.79 cal mol^{-1} K^{-1} using scaled and unscaled frequencies, respectively. The agreement between the experimental $\Delta S^{\ddagger}_{298}$, −3.3(0.4) cal mol^{-1} K^{-1}, and calculated values is good and indicates that a statistical model of the kinetics of the Berry pseudorotation process may be valid.

3. Kinetics. This part compares the pressure-dependent rate constants obtained in the present study and those obtained in our earlier study with RRKM predictions which employed results of the theoretical calculations described in the preceding section. Effects of weak collisions and non-RRKM kinetics are also investigated.

RRKM Calculations. RRKM theory assumes that intramolecular vibrational energy redistribution (IVR) in reacting molecules is ergodic and occurs at rate constants which exceed the RRKM rate constant for the process where activated molecules, in the absence of collisions, form the transition state.[8] The energy-specific RRKM rate constant, $k_{RRKM}(E)$, is

$$k_{RRKM}(E) = \frac{LZ^{\ddagger}G^{\ddagger}(E-E_0)}{\hbar Z\rho(E)} \qquad E > E_0 \tag{1}$$

where E_0 is the critical energy, L is the statistical factor, $G^{\ddagger}(E-E_0)$ is the sum of the states in the transition state, $\rho(E)$ is the density of states of the reactant, and $\hbar$ is Planck's constant.[8] $Z^{\ddagger}/Z$ is the ratio of the adiabatic partition functions which in this case are the rotational partition functions excluding symmetry numbers. The concentration-dependent unimolecular rate constant is

$$k_{uni}([M]) = \frac{L^{\ddagger}Z^{\ddagger}\exp(-E_0/kT)}{\hbar Z}\int_{E_0}^{\infty}\frac{G^{\ddagger}(E-E_0)\exp(-E/kT)}{1+k_{RRKM}(E)/k_2[M]}\,dE \tag{2}$$

where $k_2[M]$ is the collision frequency.

The reactant $\rho(E)$ and Z were calculated from experimental data.[11,22] Since HF/6-31+G* calculations best reproduced the experimental structure and vibrational frequencies of ground-state SF_4, this level of theory was used to calculate parameters for the transition state. HF/6-31+G* transition-state vibrational frequencies multiplied by 0.893 were used to calculate $G^{\ddagger}(E-E_0)$. Since the experimental ground-state rotational constants are only ca. 1% smaller than those calculated at the HF/6-31+G* level, unscaled HF/6-31+G* rotational constants were used to

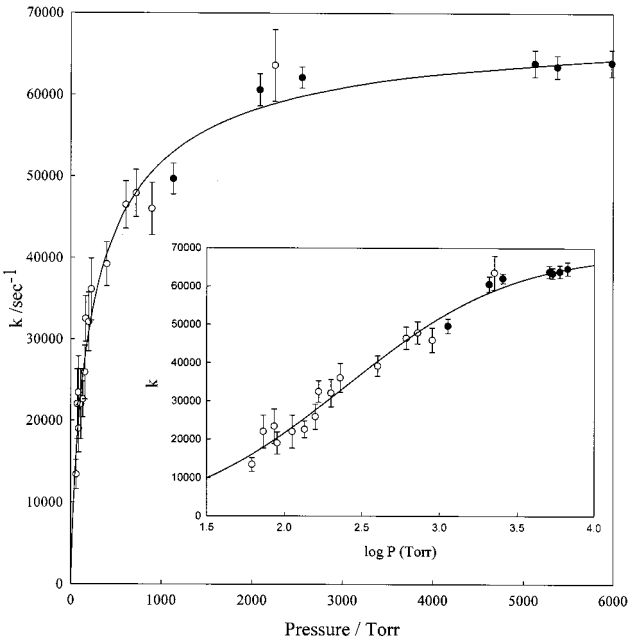

Figure 3. Experimental and calculated pressure-dependent rate constants for Berry pseudorotation of SF_4 at 335 K. Data reported in ref 6 are designated by open circles, and data obtained in the present study are designated by closed circles. All calculations used $E_0 = 11.7$ kcal mol^{-1} and other parameters described in the text. The solid curve was calculated using the strong collision model with $\sigma_{HS} = 4$ Å. The main figure shows data plotted as k/s^{-1} vs P/Torr, and the inset shows data plotted as k/s^{-1} vs log(P/Torr).

calculate $Z^{\ddagger}$. The statistical factor, L, is the ratio of the rotational symmetry number of the reactant to that of the transition state.[30,31] The reactant and transition state have C_{2v} and C_{4v} symmetry, respectively, and L is therefore $^1/_2$ for the Berry pseudorotation process of SF_4. $G^{\ddagger}(E-E_0)$, $\rho(E)$, and $k_{RRKM}(E)$ values were calculated at 25 cm^{-1} increments from E_0 to $E_0 +$ 5000 cm^{-1} using the direct count procedure. The falloff was calculated using a program written by Hase et al.[32] and also using the RRKM program from the UNIMOL program suite.[18] A reactant molecule is "activated" when its E exceeds E_0. For $E_0 = 11.7$ kcal mol^{-1}, the average energy of an activated molecule, $\langle E-E_0\rangle$, is 0.91 kcal mol^{-1}, its average state density, $\langle\rho(E)\rangle$, is 48 states/cm^{-1}, and its $\langle k_{RRKM}(E)\rangle$ is 7.4×10^8 s^{-1}.

Using a Lennard-Jones (LJ) collision frequency instead of a hard sphere collision frequency has little effect on the shape of the strong collision falloff curve; i.e., the shape is not very sensitive to whether a hard sphere or LJ collision model is used. For example, pressure-dependent rate constants calculated at 335 K between 0.001 and 1×10^6 Torr using a hard sphere collision frequency with a hard sphere collision diameter, σ_{HS}, of 4 Å differ by 1% or less from those calculated using a LJ collision frequency calculated with a LJ collision diameter, σ_{LJ}, of 2.9 Å and a well depth, ϵ/k (k is Boltzmann's constant), of 500 K.

The critical energy, E_0, and collision parameters were varied to provide the best fit of the experimental falloff curves at all temperatures where pressure-dependent rate constants were obtained. Figure 3 compares combined rate constants obtained at 335 K and results of RRKM calculations. The earlier data, reported to be at 336 K, fit smoothly with the data obtained in the present study at 335 K. The solid curve in Figure 3 shows results of RRKM calculations using the input parameters described above with a collision diameter, σ_{HS}, of 4 Å and a critical energy, E_0, of 11.7 kcal mol^{-1}. This calculation reproduces the curvature and displacement of the experimental falloff. These parameters also yield calculated rate constants that agree with experimental values obtained previously at ca. 306, 328, and 348 K. Different sets of parameters can also fit the data at one or more temperatures, but this set provides the best fit at all four temperatures where data were obtained.

An E_0 of 11.7 kcal mol^{-1} and a σ_{HS} of 4 Å or $\sigma_{LJ} = 2.9$ Å and $\epsilon/k = 500$ K are reasonable for this system. The experimental E_∞, 11.9(0.2) kcal mol^{-1}, is consistent with $E_0 = 11.76$-(0.20) kcal mol^{-1} calculated using average internal energies of the ground and transition states calculated at the HF/6-31+G* level.[8] The hard sphere diameter of SF_4 is ca. 4 Å, assuming van der Waals atomic radii. The rotationally inelastic collision diameter, determined from ^{19}F T_1 measurements, is ca. 2.19 Å at 335 K.[33] LJ parameters for SF_4 have not been reported. The intermolecular potential for SF_6, however, has been determined from collision-induced light scattering spectra, viscosity measurements, and virial coefficient data, and σ has been reported to be between 4.6 and 5 Å and ϵ/k between 300 and 500 K.[34,35] It is reasonable to assume that σ_{LJ} for SF_4 is somewhat smaller and ϵ/k is comparable or larger since SF_4 is slightly polar. Ab initio molecular orbital calculations of the energy of a SF_4-SF_4 collision complex as a function of the distance between the two S atoms were performed at the HF/6-31G* level. For the minimum energy approach, ϵ/k is ca. 1200 K and the σ is ca. 4 Å. Averaging over all approach orientations would reduce ϵ/k due to contributions of approach angles which involve dipole−dipole repulsion.

The lack of acceptable agreement between our earlier experimental and RRKM calculated rate constants can be attributed to several factors. Both the experimental E_∞ and A_∞ values were significantly different from those of the present study. The RRKM calculations used an E_∞ too high and an unrealistic model for the transition state which reproduced A_∞. Reduced plots (k/k_∞) were used in the analysis as is customarily done, but because the rate constants obtained at 2004 Torr were assumed to be k_∞ values, the reduced falloff plots exhibited less curvature.

Given the scatter in the experimental data and the number of parameters required to calculate RRKM rate constants and their uncertainties, it is important to investigate whether the data could also fit a weak collision model and/or be consistent with some degree of non-RRKM behavior. These topics are addressed below.

Weak Collision Effects. RRKM analysis is based on the strong collision assumption, i.e., that collisional energization and de-energization are single-step processes. When this is not the case, rate constants for collisional energy transfer determine the curvature of the falloff.[8,36] Effects of stepwise collisional energy transfer on the shape of the falloff for Berry pseudorotation of SF_4 were investigated using the UNIMOL program suite[18] which employs an energy-grained master equation to calculate rate constants. Gilbert et al. have shown that the falloff depends primarily on the average energy transferred per collision and is not very sensitive to the complete form of the collisional energy transfer probability distribution function.[36]

In contrast to the strong collision model, the curvature of weak collision falloff curves is sensitive to the collision model employed in the calculation. Using the LJ model, increasing ϵ/k makes the falloff curve closer to the shape calculated using the strong collision assumption. The LJ model is a more accurate representation of collisions at the low temperatures used in the present study and was used in all weak collision calculations. Falloff curves were calculated using the "exponential down" model for values of the average energy lost by an activated

molecule per collision, $\langle\Delta E_{down}\rangle$, of 500, 1000, 1500, and 2000 cm^{-1}.[36] The values of all other parameters were the same as those used in the strong collision calculations described above. Decreasing the value of $\langle\Delta E_{down}\rangle$ displaces the falloff curves to higher pressure and also increases the pressure range required for the complete transition from first- to second-order kinetics. The LJ parameters required to generate falloff curves which reproduce the experimental data at 335 K were determined for $\langle\Delta E_{down}\rangle$ values of 2000, 1500, 1000, and 500 cm^{-1}. The calculated falloff curves for $\langle\Delta E_{down}\rangle = 2000$, 1000, and 1500 cm^{-1} are almost indistinguishable from the strong collision falloff curve shown in Figure 3 and provide an acceptable fit of the experimental rate constants for $\langle\Delta E_{down}\rangle = 500$ cm^{-1}; the curvature of the calculated falloff curve does not provide as good a fit of the experimental data. Using $\epsilon/k = 500$ K, the best agreement is obtained for $\langle\Delta E_{down}\rangle$ values of 2000, 1500, 1000, and 500 cm^{-1}, with σ_{LJ} values of 3.5, 4, 4.5, and 5.5 Å, respectively. Increasing ϵ/k to 1000 K reduces the σ_{LJ} values required to fit the data by ca. 0.5 Å for the range of $\langle\Delta E_{down}\rangle$ values used. Reducing ϵ/k to 250 K increases the σ_{LJ} values required to fit the data by ca. 0.5 Å for the range of $\langle\Delta E_{down}\rangle$ values used. These calculations show that the weak collision model also fits the experimental rate constant data for a range of $\langle\Delta E_{down}\rangle$ values combined with various σ_{LJ}. The σ_{LJ} and ϵ/k values required to match the experimental data for $\langle\Delta E_{down}\rangle =$ 500 and 1000 cm^{-1} appear large on the basis of comparison with reported values for SF_6.[33,34] It can be concluded that the weak collision model can also adequately reproduce the experimental data for large $\langle\Delta E_{down}\rangle$ values.

At the low temperature, 335 K, where experimental rate constants were obtained, it is reasonable that most collisions between activated and thermally averaged SF_4 molecules would be strong. This low temperature facilitates single-step deactivation because most of the activated molecules have energies close to E_0 and collision durations are long. The distribution function of activated SF_4 molecules, i.e., those with internal energies above E_0, was calculated assuming a Boltzmann distribution and using direct count state densities. At 335 K, for $E_0 = 11.7$ kcal mol^{-1}, the average vibrational energy of an activated SF_4 molecule is ca. 280 cm^{-1} above E_0 and only ca. 20% of the activated molecules have energies more than 500 cm^{-1} above E_0. At 335 K, the average duration of a collision between two SF_4 molecules is 1.5×10^{-12} s using $\sigma_{LJ} = 3$ Å and $\epsilon/k = 500$ K. This time is long compared to the time required to execute a complete vibration, indicating that it is likely that $\langle\Delta E_{down}\rangle$ is several kcal mol^{-1} for a collision between an activated SF_4 molecule with $E = 12.9$ kcal mol^{-1} and a typical SF_4 molecule with an average vibrational energy of 1.0 kcal mol^{-1}.[37-39]

Non-RRKM Effects. First of all, it is important to note that some non-RRKM effects will not produce significant changes in RRKM calculated falloff curves and the data obtained in the present study are not sensitive to them. Competition between energy-specific reaction rate constants, $k_{eff}(E)$ values, and collision rate constants determines the curvature and location of the falloff curve. The RRKM energy-specific rate constant, $k_{RRKM}(E)$ (eq 1), is calculated assuming the total density of states, $\rho(E)$, and the total sum of transition-state states, $G^{\ddagger}(E-E_0)$, are available to the reacting molecule. Consider an equation similar to eq 1 for $k_{eff}(E)$ where the $\rho(E)$ and $G^{\ddagger}(E-E_0)$ values can be less than the RRKM values. Equation 1 shows that the RRKM energy-specific rate constant, $k_{RRKM}(E)$, depends on the $G^{\ddagger}(E-E_0)/\rho(E)$ ratio. $G^{\ddagger}(E-E_0)$ and $\rho(E)$ can depart from their RRKM values and $k_{eff}(E)$ will still equal $k_{RRKM}(E)$ provided that the $G^{\ddagger}(E-E_0)/\rho(E)$ ratio is maintained at the RRKM value for all values of E. This would occur if, for example, 20% of the state density of the reactant and 20% of the states of the transition state do not participate in the reaction. The present experiments are also not very sensitive to a second type of non-RRKM behavior which will affect the displacement of the falloff curve without changing its shape. If all the states of the transition state are reactive, but only a certain fraction of activated molecules react, all the $k_{eff}(E)$ will increase by the same factor without changing the shape of the falloff curve and a larger collision diameter will be required to fit the experimental data. For example, if 20% of the state density is nonreactive, the average energy-specific rate constant, $\langle k_{eff}(E)\rangle$ increases from 7.4×10^8 s^{-1} (which is $\langle k_{RRKM}(E)\rangle$ for Berry pseudorotation of SF_4) to 8.9×10^8 s^{-1}, displacing the falloff curve to higher pressures without changing its curvature. This requires a collision diameter which is only ca. 10% larger. The collision diameter of SF_4 is not well determined, and non-RRKM behavior of this type and magnitude cannot be ruled out by the present data.

In principle, pressure-dependent rate constants are sensitive to non-RRKM effects which cause changes in the shape of the calculated falloff curve. The shape of the falloff will deviate from RRKM predictions if IVR in some activated states is slow but not negligible.[40] Equation 1 will not provide accurate $k_{eff}(E)$ values in this case. The total state density can, in principle, be divided into grains, each with its own IVR rate, which for some grains will be rate limiting and therefore equal to $k_{eff}(E)$. Each grain will contribute to the falloff curve with a different pressure dependence. The contribution from grains with smaller $k_{eff}(E)$ increases with decreasing pressure. It was noted by Bauer et al.[7] that k/P was increased with decreasing pressure at the lowest pressures where Berry pseudorotation rate constants were obtained for SF_4. This was attributed to this type of non-RRKM behavior and that reactions of molecules with excitation in regions of vibrational phase space weakly coupled to the reaction coordinate were able to react due to the increasing time between deactivating collisions. The RRKM calculations performed in the present study indicate that the bimolecular region is at pressures below 0.1 Torr for this process. All the experimental rate constants were in the falloff region. In fact, only a few rate constants were obtained below $P_{1/2}$, the pressure where the unimolecular rate constant is reduced to $^1/_2$ its limiting high-pressure value. Plotting the data shown in Figure 3 as k/P vs P does not reveal a departure from RRKM predictions at low P. The experimental data are very scattered at the low pressures, but the general shape of the experimental falloff is in agreement with the RRKM calculations with the k/P values increasing with decreasing P in this region.

A major result of this study is that the RRKM model and the strong collision assumption can successfully predict the location with respect to pressure and the curvature of the experimentally determined falloff curve for Berry pseudorotation of SF_4. Weak collision calculations also provide an acceptable model for large values for the average energy transferred per collision. If deviations from RRKM kinetics do occur for this process, their magnitude is not great enough to significantly perturb the observed falloff curves from the shape predicted by RRKM theory. For experimental data of the quality obtained in the present study and in most studies which have measured unimolecular falloff curves, non-RRKM effects would have to be large and of a type which significantly changes the $k_{eff}(E)$ values, to be detectable. Measurable differences in the shape of the observed falloff from that calculated from strong collision RRKM theory were not observed, and unreasonably large

collision parameters were not required to make the calculated and observed falloff curves coincide.

There is a reason, aside from model insensitivity, why RRKM theory provides an acceptable model for this process. IVR in activated SF_4 molecules may be ergodic or nearly so. For all energized molecules to contribute in a statistical sense to the macroscopic rate constant, IVR must be ergodic and occur on time scales which are short compared to $1/(k_{RRKM}(E))$. Assuming a Boltzmann distribution of reacting molecules, the average activated molecule has $\langle E-E_0\rangle = 0.91$ kcal mol^{-1}, and $\langle k_{RRKM}(E)\rangle = 7.40 \times 10^8$ s^{-1}. The average time for an activated molecule to react is 1.35×10^{-9} s, a time long enough for it to execute thousands of vibrations. The lifetime, $\tau(E)$, of a vibrational state in the absence of collisions and radiative processes is governed by the Fermi Golden rule, as applied to IVR processes, $\tau(E) = 1/\langle k_{IVR}(E)\rangle = [(2\pi/\hbar)\rho(E)\times f4H_{mn}\times f4^2]^{-1}$, where H_{mn} is the average coupling matrix elements between the states. For the kinetics to be statistical or nearly so $\langle k_{ivr}\rangle \gg \langle k_{RRKM}(E)\rangle$. Since the average total state density of an activated SF_4 molecule is 48/cm^{-1}, this condition requires the matrix elements coupling the excited vibrational states to be greater than 0.01 cm^{-1}, which is not unreasonable for Coriolis coupling constants and anharmonic coupling constants at the level of vibrational excitation of a typical activated SF_4 molecule.[41]

Conclusions

The conclusions of this study are the following: (1) The strong collision RRKM model as applied to Berry pseudorotation of SF_4 reproduces the experimentally determined falloff curve. The combination of scatter in the experimental data and uncertainties in collision parameters employed in the calculations and model insensitivity makes it impossible to rule out the presence of a small degree of weak collisional effects and some non-RRKM effects. (2) Since the process can be modeled with RRKM theory, it is valid to apply transition state theory to the high-pressure rate constants. (3) Full geometry optimization ab initio calculations at the HF and MP2 levels using the 6-311+G** basis set adequately reproduce all the experimentally determined activation parameters for the process. MP4/6-31+G* single-point energy calculations at the HF/6-31+G* optimized geometry also predict activation parameters close to the experimental values. (4) DFT calculations using the B3LYP and B3PW91 hybrid density functionals and the HF/6-31+G* reproduce the experimental data less well. (5) Earlier reports which concluded that this process was not RRKM were based on inaccurate values of the E_{act} most likely due to small systematic errors in temperature measurement as well as the lack of a realistic model for the transition state.

Acknowledgment. This research was supported by the National Science Foundation (Grant CHE 93-21079) and the Committee on Research of the University of California, Davis.

References and Notes

(1) Klemperer, W. G.; Krieger, J. K.; McCreary; Muetterties, E. L.; Traficante, D. D.; Whitesides, G. M. *J. Am. Chem. Soc.* **1975**, *97*, 7023.

(2) (a) Berry, R. S. *J. Chem. Phys.* **1960**, *32*, 933. (b) Berry, R. S. *Rev. Mod. Phys.* **1960**, *32*, 447.

(3) LeMaster, C. B. *Prog. Nucl. Magn. Reson. Spectrosc.* **1997**, *31*, 119.

(4) True, N. S.; Suarez, C. *Advances in Molecular Structure Research*; JAI Press: New York; 1995; pp 115−155.

(5) True, N. S. In *Encyclopedia of NMR;* Grant, D. M., Harris, R. K., Eds.; John Wiley and Sons: Chichester, England, 1996; p 2173.

(6) Spring, C. A.; True, N. S. *J. Am. Chem Soc.* **1983**, *105*, 7231.

(7) Bauer, S. H.; Lazaar, K. I. *J. Chem. Phys.* **1983**, *79*, 2808.

(8) Holbrook, K. A.; Pilling, M. J.; Robertson, S. H. *Unimolecular Reactions*, John Wiley and Sons: Chichester, England, 1996.

(9) Wiberg, K. B.; Rablen, P. R.; Rush, D. J.; Keith, T. A. *J. Am. Chem. Soc.* **1995**, *117*, 4261.

(10) LeMaster, C. L.; LeMaster, C. B.; True, N. S. *J. Am. Chem. Soc.* **1999**, *121*, 4478.

(11) Irikura, K K. *J. Chem. Phys.* **1995**, *102*, 5357.

(12) Baird, N. C.; Taylor, K. F. *Can. J. Chem.* **1981**, *59*, 814.

(13) Minyaev, R. R.; Yudilevich, J. A. *J. Mol. Struct.: THEOCHEM* **1992**, *262*, 73.

(14) Seel, F.; Bundenz, R.; Werner, D. *Chem. Ber.* **1964**, *97*, 1369.

(15) (a) Stephenson, D. S.; Binsch, G. Program No. 365, Quantum Chemistry Program Exchange, Indiana University, Bloomington, IN 47405. (b) LeMaster, C. B.; LeMaster, C. L.; True, N. S. Program No. 569 and QCMP059, Quantum Chemistry Program Exchange, Indiana University, Bloomington, IN 47405.

(16) Frisch, M. J.; Trucks, G. W.; Schlegel, H. B.; Gill, P. M. W.; Johnson, B. G.; Robb, M. A.; Cheeseman, J. R.; Keith, T.; Petersson, G. A.; Montgomery, J. A.; Raghavachari, K.; Al-Laham, M. A.; Zakrzewski, V. G.; Ortiz, J. V.; Foresman, J. B.; Peng, C. Y.; Ayala, P. Y.; Chen, W.; Wong, M. W.; Andres, J. L.; Replogle, E. S.; Gomperts, R.; Martin, R. L.; Fox, D. J.; Binkley, J. S.; Defrees, D. J.; Baker, J.; Stewart, J. P.; Head-Gordon, M.; Gonzalez, C.; Pople, J. A.; Gaussian 94, Revision B.2, Gaussain, Inc., Pittsburgh, PA, 1995.

(17) Hase, W. L.; Bunker, D. L. Program No. 234, Quantum Chemistry Program Exchange, Indiana University, Bloomington, IN 47405.

(18) Gilbert, R. G.; Smith, S. C.; Jordan, M. J. T. UNIMOL program suite (calculation of falloff curves for unimolecular and recombination reactions), 1993. Available from the authors at the School of Chemistry, Sydney University, NSW 2002, Australia, or by e-mail to gilbert_r@summer.chem.su.oz.au.

(19) Tossell, J. A.; Lazzeretti, P. *J. Chem. Phys.* **1988**, *88*, 7251.

(20) Seel, F.; Gombler, W. *J. Fluorine Chem.* **1974**, *4*, 331.

(21) The pressures reported refer to the pressure at the filling temperature, 298 K. The ideal gas law was used to calculate the pressures at 335 K.

(22) Tolles, W. M.; Gwinn, W. D. *J. Chem. Phys.* **1962**, *36*, 1119.

(23) Hu, C. H.; Chong, D. P. *Encyclopedia of Computational Chemistry;* von Rogue Schleyer, P., Ed.; John Wiley and Sons: New York, 1998; pp 664−678.

(24) Altmann, J. A.; Handy, N. C.; Ingamells, V. E. *Int. J. Comput. Chem.* **1996**, *57*, 533.

(25) Scott, A. P.; Radom, L. *J. Phys. Chem.* **1996**, *100*, 16502.

(26) Wong, M. W. *Chem. Phys. Lett.* **1996**, 391.

(27) Levin, I. W.; Harris, W. C. *J. Chem. Phys.* **1971**, *55*, 3048.

(28) Note the Gaussian 94 designation of the B_1 and B_2 irreducible representations of C_{4v} is reversed from that in many texts.

(29) The activation entropy $\Delta S^{\ddagger}_{298}$ is $S^{\ddagger} - S_{reactant}$. The calculated S of the reactant in the pseudorotation process is not the same as the S of ground-state SF_4. The reactant is isolated to one well of the double minimum pseudorotation potential function, and its entropy is lower than the total entropy of the ground state by a factor of R ln 2 because it can only access the states in the other well via reaction.

(30) Pollak, E.; Pechukas, P. *J. Am. Chem. Soc.* **1978**, *100*, 2984.

(31) Coulson, D. R. *J. Am. Chem. Soc.* **1978**, *100*, 2992.

(32) Hase, W. L. Private communication.

(33) Spring, C. A.; True, N. S. *J. Magn. Reson.* **1984**, *58*, 338.

(34) Meiander, N. *J. Chem. Phys.* **1993**, *99*, 8654.

(35) Aziz, R. A., Slamam, M. J.; Taylor, W. L.; Hurly, J. J. *J. Chem. Phys.* **1991**, **94**, 1034.

(36) Gilbert, R. G.; Smith, S. C. *Theory of Unimolecular and Recombination Reactions;* Blackwell Scientific Publications: Oxford, England, 1990.

(37) Oref, I.; Tardy, D. C. *Chem. Rev.* **1990**, *90*, 1407.

(38) Tardy, D. C., Rabinovitch, B. S. *Chem. Rev.* **1977**, *77*, 369.

(39) Flynn, G. W.; Parmenter, C. S.; Wodtke, A. M. *J. Phys. Chem.* **1996**, *100*, 12817.

(40) Pritchard, H. O. *The Quantum Theory of Unimolecular Reactions*; Cambridge University Press: Cambridge, England, 1984.

(41) Christen, D. *J. Mol. Spectrosc.* **1992**, *151*, 1.